Surface segregation of ternary alloys
Effect of the interaction between solute elements

Zhao, Meng; Brouwer, Johannes C.; Sloof, Willem G.; Bottger, Amarante

DOI
10.1002/admi.201901784

Publication date
2020

Document Version
Final published version

Published in
Advanced Materials Interfaces

ADVANCED MATERIALS INTERFACES
www.advmatinterfaces.de

Surface Segregation of Ternary Alloys: Effect of the Interaction between Solute Elements

*Meng Zhao, Johannes C. Brouwer, Willem G. Sloof, and Amarante J. Böttger**

Ternary alloys have been developed for a wide range of applications and surface segregation of ternary alloys has a decisive impact on their performance. Different from binary alloys, in which surface energy is usually the dominant factor, the interaction between solute elements has a noticeable effect on the surface segregation behavior of ternary alloys. As a practical example, Pd-based ternary alloys have been proposed as promising candidates for hydrogen separation membranes due to their excellent permeability and selectivity. In the present work, surface segregation of Pd-Cu-Ag and Pd-Cu-Mo ternary alloys in both vacuum and hydrogen atmosphere is investigated. X-ray photoelectron spectroscopy and low energy ion scattering spectroscopy analyses reveal that the segregation trend of the outermost atomic layer is not always the same as that of the near-surface region. A thermodynamic model is developed to describe the surface segregation of ternary alloys. The results of the model are in good qualitative agreement with experimental results. Furthermore, calculations for other ternary alloy systems confirm that the model provides a simple but universal method for surface segregation in ternary alloys. The results can also be considered as basic guidelines to design novel ternary alloys for various applications.

1. Introduction

Alloys, consisting of a matrix solvent element and an additive solute element, are fundamental and versatile material systems, dating from bronze wares in ancient time until the numerous products in modern industries.[1–3] Beside the academic challenge of crossing the binary barrier, ternary alloys have gained more and more attention as they may have outstanding properties as structural and functional components in various applications. For example, stainless steel containing 18–20 at% of chromium and 8–10.5 at% of nickel is used for constructions, machinery, and vehicle components.[4] Ni-Al-X (X: Re, W) ternary alloys are crucial for aircraft engines operating under extreme conditions.[5] III–V ternary alloys are important semiconductors for electronic industries.[6] Ternary alloys of noble metals (Pt, Rh, Pd, Au, etc.) are also widely used as catalysts for energy, chemical engineering, and environmental applications.[7]

In general, the catalytic performance of ternary alloys is dominated by the elemental composition and atomic structure at the surface.[8] Therefore, surface segregation has a strong impact on the activity and stability of ternary alloy catalysts.[9] As a typical case, palladium-based alloys have the potential to play an important role in virtually every aspect of the envisioned hydrogen economy, because of their excellent hydrogen dissociation and absorption properties.[10] Therefore, the application of Pd or Pd-alloy membranes is currently the most promising for separation and purification for hydrogen production from natural gas in membrane reactors.[11,12] Except of its high price, the major drawback of Pd membranes is the hydrogen embrittlement caused by the metal/hydride (α/β) phase transition under the process conditions.[13] This problem can be solved by alloying Pd with metal atoms with larger atomic sizes.[14] For example, in Pd-Ag alloy, the lattice expansion by Ag atoms reduces the effect of hydrogen absorption.[15] Also, Pd-based ternary alloys have been developed with higher hydrogen permeability and better corrosion resistance.[9,16] However, surface segregation deteriorates the long-term hydrogen dissociation performance of Pd-alloy membranes.[17,18] Therefore, understanding of driving forces and influencing factors of surface segregation is of great importance to improve the performance of Pd-based alloys for hydrogen separation membranes.

So far, experimental investigations of surface segregation of Pd-based ternary alloys are confined to a few systems. For example, surface segregation of Pd-Cu-Ag was investigated by X-ray photoelectron spectroscopy (XPS).[19,20] Low energy ion scattering spectroscopy (LEISS) was adopted to investigate the surface segregation of Pd-Cu-Au.[21] However, the surface segregation of a ternary alloy in both vacuum and a gas atmosphere has never been systematically investigated and discussed.

Most research addressed surface segregation of binary alloys, and has already provided good results for Pd-based binary alloys.[22,23] Pioneering work on surface segregation of ternary alloys has been performed by Guttmann based on statistical thermodynamics of adsorption isotherms.[24] Hoffmann and Wynblatt refined Guttmann's approach and gave

Dr. M. Zhao, J. C. Brouwer, Dr. W. G. Sloof, Dr. A. J. Böttger
Department of Materials Science and Engineering
Delft University of Technology
Mekelweg 2, 2628 CD Delft, The Netherlands
E-mail: A.J.Bottger@tudelft.nl

The ORCID identification number(s) for the author(s) of this article can be found under https://doi.org/10.1002/admi.201901784.

DOI: 10.1002/admi.201901784

an analytical derivation.[25] However, Guttmann's model considers the reduction of surface energy as the only driving force of the segregation, regardless of the chemical bonding between constituting elements. In Wynblatt's model, in addition, elastic strain energy is taken into consideration, but a gas atmosphere, was not included.[26] Monte Carlo simulation based on modified embedded atom method studies of surface segregation is also performed, mostly applying to in vacuum condition.[27,28] As already shown for binary alloys used for hydrogen separation, both hydrogen adsorption on the surface and absorption in the bulk may affect the thermodynamic equilibrium state, thus changing the surface segregation behavior.[29,30] Yet, the surface segregation of Pd-based ternary alloys in both vacuum and hydrogen atmosphere is not well studied and understood.

In the present work, Pd-Cu-Ag and Pd-Cu-Mo alloys were selected for surface segregation investigation, as they potentially could be used in hydrogen separation membranes. Surface segregation was investigated in both vacuum and hydrogen gas atmosphere by XPS and LEISS, thereby probing different depths below the surface. Besides that, a thermodynamic model was developed based on the atom exchange approach to understand and predict surface segregation of ternary alloys in vacuum and in hydrogen gas atmosphere. The interaction between solute elements in ternary alloys and the role of the hydrogen gas atmosphere were investigated.

2. Thermodynamic Modeling

2.1. Equilibrium Segregation of the Outermost Atomic Layer

Surface segregation of ternary alloy M-A-B (M is the solvent element, which is Pd here, while A and B are two different solute elements) can be expressed as[25]

$$\frac{x_i^{\mathrm{surf}}}{1-x_i^{\mathrm{surf}}-x_j^{\mathrm{surf}}}=\frac{x_i^{\mathrm{bulk}}}{1-x_i^{\mathrm{bulk}}-x_j^{\mathrm{bulk}}}\exp\left(-\frac{\Delta H_i^{\mathrm{seg}}}{RT}\right)\quad (i,j=\mathrm{A,B}) \tag{1}$$

where x_i^{surf} is atomic fraction of solute element in the outermost atomic layer, x_i^{bulk} is bulk atomic fraction, T is the absolute temperature at which the equilibrium is obtained, and R is the gas constant. The effect of segregation enthalpy is considered in the exponent part, while the effect of entropy is implied by the atomic fraction at the surface and in the bulk of the alloy as a standard solution. Notably, only configurational entropy is taken into consideration, while effect of vibrational and electronic entropy is neglected. Consequently, when $\Delta H_{\mathrm{seg}} < 0$, segregation of solute will occur, and when $\Delta H_{\mathrm{seg}} > 0$, segregation of solvent will occur.

2.2. Segregation Enthalpy: Atom Exchange Approach in Vacuum and Hydrogen

2.2.1. Segregation in Vacuum

ΔH^{seg} can be determined by atom exchange between the outermost surface and the bulk.[3] Therefore, ΔH^{seg} is mainly determined by the change of configurational energy during atom exchange and the related elastic strain energy[25]

$$\begin{aligned}\Delta H_i^{\mathrm{seg}}=&(\gamma_i\sigma_i-\gamma_{\mathrm{M}}\sigma_{\mathrm{M}})+2\omega_{i\mathrm{M}}\left[Z_{\mathrm{l}}\left(x_i^{\mathrm{bulk}}-x_i^{\mathrm{surf}}\right)+Z_{\mathrm{v}}\left(x_i^{\mathrm{bulk}}-\frac{1}{2}\right)\right]\\&+\omega'\left[\left(x_j^{\mathrm{surf}}-x_j^{\mathrm{bulk}}\right)-Z_{\mathrm{v}}x_j^{\mathrm{bulk}}\right]-\Delta H_{i\mathrm{M}}^{\mathrm{elastic}}\end{aligned} \tag{2}$$

where the subscript i, j = A, B represent the corresponding elements. γ is the surface energy of pure metals, and σ is the atomic surface area related to the atomic volume. Z_{l} and Z_{v} are numbers of nearest lateral and vertical neighbors, respectively. ω is the alloy parameter, which is related to the mixing enthalpy (ΔH^{mix}) of the so-called "sub-binary alloys," A-M, B-M, and A-B, in the ternary alloy

$$\omega_{ij}=\frac{\Delta H_{ij}^{\mathrm{mix}}}{Zx_ix_j},\quad i,j=\mathrm{A,B,M} \tag{3}$$

where $Z = Z_{\mathrm{l}} + 2Z_{\mathrm{v}}$ is the total number of nearest neighbors and x_i (x_j) is the atomic fraction of the corresponding element. For example, Z is 12 for FCC Pd-based alloys. For ternary alloys, ω' is related to the alloy parameter of the three sub-binary alloys by

$$\omega'=\omega_{\mathrm{AB}}-\omega_{\mathrm{AM}}-\omega_{\mathrm{BM}} \tag{4}$$

The calculation of the mixing enthalpy of the sub-binary alloys will be introduced in Section 2.3, where an extension of Miedema's model is also proposed.

The elastic strain energy ($\Delta H_{ij}^{\mathrm{elastic}}$) was calculated according to[3]

$$\Delta H_{ij}^{\mathrm{elastic}}=\frac{2K_iG_j\left(V_i-V_j\right)^2}{3K_iV_j+4G_jV_i} \tag{5}$$

where K_i, G_i, and V_i represent the bulk modulus, shear modulus, and molar volume of the corresponding metal i, respectively.

2.2.2. Segregation in Hydrogen Atmosphere

The effect of hydrogen adsorption on the surface and absorption in the bulk on the segregation enthalpy can be included as[23]

$$\begin{aligned}\Delta H_i^{\mathrm{seg}}=&(\gamma_i\sigma_i-\gamma_{\mathrm{M}}\sigma_{\mathrm{M}})+2\omega_{i\mathrm{M}}\left[Z_{\mathrm{l}}\left(x_i^{\mathrm{bulk}}-x_i^{\mathrm{surf}}\right)+Z_{\mathrm{v}}\left(x_i^{\mathrm{bulk}}-\frac{1}{2}\right)\right]\\&+\omega'\left[Z_{\mathrm{l}}\left(x_j^{\mathrm{surf}}-x_j^{\mathrm{bulk}}\right)-Z_{\mathrm{v}}x_j^{\mathrm{bulk}}\right]-\Delta H_{i\mathrm{M}}^{\mathrm{elastic}}+\theta(\varepsilon_i-\varepsilon_{\mathrm{M}})\\&+Z_{\mathrm{v}}x_{\mathrm{H}}\left(\Delta H_{\mathrm{H\ in\ M}}^{\mathrm{sol}}-\Delta H_{\mathrm{H\ in}\ i}^{\mathrm{sol}}\right)\end{aligned} \tag{6}$$

where θ is the adsorption coverage of H atoms on the surface (the molar ratio between hydrogen atoms adsorbed on the surface and the total surface metal atoms), ε_i is the adsorption energy of the corresponding solute element i. In the present work, a hydrogen atmosphere is considered, adsorption of other gas molecules can also be included by adapting the adsorption energy ε_i and θ. x_{H} is the concentration of absorbed

H atoms in the bulk (the molar ratio between hydrogen atoms absorbed in the bulk and the total metal atoms) and $\Delta H^{\mathrm{sol}}_{\mathrm{H\,in}\,i}$ is the formation enthalpy of the corresponding metal hydride.

2.3. Mixing Enthalpy: Extended Miedema's Model

Miedema's model has been successfully applied to calculate the mixing enthalpy of binary alloys of transition metals.[3] Most of previous calculations of mixing enthalpies of ternary alloys are made by means of extrapolation from sub-binary alloys.[31] For example, Zhang and Jesser developed a model using the mole-fraction weighted average of mixing enthalpy of sub-binary alloys to obtain those of ternary alloys; configurational energy and elastic strain energy were both considered.[32] However, it was not clear how to asymmetrically select the solute and solvent elements in the alloy. Ouyang et al. reported a so-called "geometric Miedema's model" (GMM) to symmetrically deal with the sub-binary alloy couples and then calculated the mixing enthalpy of Fe-Al-RE ternary alloys.[33] In both models, the effect of the third element on the selected sub-binary system was not included. To overcome this issue, a "two-step Miedema's model" (TSMM) was proposed by Wang et al.: first calculate the mixing enthalpy of the sub-binary alloy A-B, considering it as a new "binary" element $\overline{\mathrm{AB}}$, with the atomic fraction weighted average properties of A and B, and then, add the effect of a third element C by another step of mixing enthalpy calculation for $\overline{\mathrm{AB}}$- C "alloy."[34] Comparing with previous models, a better estimation of the mixing enthalpy of Al-Ni-Y ternary alloys has been achieved, although the effect of elastic strain energy was simplified by a single-parameter correction.

In this work, a combination of GMM and TSMM was developed, in which both the configurational energy and elastic strain energy in the mixing enthalpy of sub-binary alloys were calculated symmetrically, while also the effect of the third element has been included.

According to the geometric model, the formation enthalpy of ternary alloys can be expressed as[33]

$$\Delta H_{\mathrm{ABM}} = \frac{x_{\mathrm{A}}x_{\mathrm{B}}}{\gamma^{\mathrm{A}}_{\mathrm{AB}}\gamma^{\mathrm{B}}_{\mathrm{AB}}}\Delta H_{\mathrm{AB}}\left(\gamma^{\mathrm{A}}_{\mathrm{AB}},\gamma^{\mathrm{B}}_{\mathrm{AB}}\right)+\frac{x_{\mathrm{A}}x_{\mathrm{M}}}{\gamma^{\mathrm{A}}_{\mathrm{AM}}\gamma^{\mathrm{M}}_{\mathrm{AM}}}\Delta H_{\mathrm{AM}}\left(\gamma^{\mathrm{A}}_{\mathrm{AM}},\gamma^{\mathrm{M}}_{\mathrm{AM}}\right) + \frac{x_{\mathrm{B}}x_{\mathrm{M}}}{\gamma^{\mathrm{B}}_{\mathrm{BM}}\gamma^{\mathrm{M}}_{\mathrm{BM}}}\Delta H_{\mathrm{BM}}\left(\gamma^{\mathrm{B}}_{\mathrm{BM}},\gamma^{\mathrm{M}}_{\mathrm{BM}}\right) \tag{7}$$

where ΔH_{ABM} is the formation enthalpy of the ternary alloy. ΔH_{AM}, ΔH_{BM}, and ΔH_{AB} are the formation enthalpies of the three sub-binary alloys. x_{A}, x_{B}, and x_{M} are the atomic fractions of corresponding elements, γ^{i}_{ij} and γ^{j}_{ij} are the atomic fractions of elements i and j in the sub-binary alloys. They can be extrapolated from the composition of ternary alloy: $\gamma^{i}_{ij}+\gamma^{j}_{ij}=1$ and $\gamma^{i}_{ij}/\gamma^{j}_{ij}=x_i/x_j$. Therefore, they were expressed as following[33]

$$\gamma^{i}_{ij}=x_i+\delta^{i}_{ij}x_k,\quad \gamma^{i}_{ij}=x_j+\delta^{i}_{ij}x_k\quad (i,j,k=\mathrm{A},\mathrm{B},\mathrm{M}) \tag{8}$$

with

$$\delta^{i}_{ij}=\frac{\lambda_i}{\lambda_i+\lambda_j},\quad \delta^{i}_{ij}=\frac{\lambda_j}{\lambda_i+\lambda_j} \tag{9}$$

and

$$\lambda_i=\left(\Delta H^{\mathrm{sol}}_{j\,\mathrm{in}\,i}-\Delta H^{\mathrm{sol}}_{k\,\mathrm{in}\,i}\right)^2 \tag{10}$$

where $\Delta H^{\mathrm{sol}}_{i\,\mathrm{in}\,j}$ is the solution enthalpy for element i in j. The latter can be easily obtained by Miedema's model for binary alloys. Then, the mixing enthalpy of the three sub-binary alloys can be calculated symmetrically as

$$\Delta H_{ij}\left(\gamma^{i}_{ij},\gamma^{j}_{ij}\right)=x_ix_j\left(f^{j}_{i}\Delta H^{\mathrm{int}}_{i\,\mathrm{in}\,j}+f^{i}_{j}\Delta H^{\mathrm{int}}_{j\,\mathrm{in}\,i}\right) \tag{11}$$

Effect of the third element can be accounted for in the same way. The model considers the sub-binary alloy as a new kind of metal with average properties of the two elements[34]

$$\Delta H_{k\,\mathrm{in}\,ij}=\left(x_i+x_j\right)x_k\left(f^{k}_{ij}\Delta H^{\mathrm{int}}_{k\,\mathrm{in}\,ij}+f^{ij}_{k}\Delta H^{\mathrm{int}}_{ij\,\mathrm{in}\,k}\right) \tag{12}$$

Finally, the mixing enthalpy of the sub-binary alloys are obtained from

$$\Delta H^{\mathrm{mix}}_{ij}=\frac{1}{3}\left(\Delta H_{i\,\mathrm{in}\,j}+\Delta H_{k\,\mathrm{in}\,ij}\right) \tag{13}$$

The contribution of elastic strain energy is considered by

$$\Delta H^{\mathrm{elastic}}_{ij}\left(\gamma^{i}_{ij},\gamma^{j}_{ij}\right)=\gamma_i\gamma_j\left(\gamma_j\Delta H^{\mathrm{elastic}}_{i\,\mathrm{in}\,j}+\gamma_i\Delta H^{\mathrm{elastic}}_{j\,\mathrm{in}\,i}\right) \tag{14}$$

3. Results

3.1. Elemental Composition and Phase Structure of the Samples

First, X-ray microanalysis with scanning electron microscopy (SEM) using energy dispersive spectrometry (EDS) confirms the elemental uniformity of both Pd alloy samples and the quantitative analysis also provides their actual composition. As shown in **Table 1**, the actual composition is quite similar with the as-designed composition. The difference is less than 1%. Besides, X-ray diffractometry (XRD) revealed that both samples are single-phase FCC (PDF 00-005-0681 ICDD, 2019) with a weak rolling texture {220}⟨112⟩. No diffraction peaks of alloying

Table 1. Composition measured by EDS and structural characteristics of the investigated samples. Both alloys have an FCC crystalline structure. The grain size and lattice constant of the samples are also listed.

Alloy	Composition [at%]				Grain size [nm]	Lattice constant [Å]
Pd-Cu-Ag	Designed value				48 ± 31	3.8450
	Pd	Cu	Ag	Mo		
	60.0	30.0	10.0	–		
	Measured value					
	Pd	Cu	Ag	Mo		
	60.6	30.3	9.1	–		
Pd-Cu-Mo	Designed value				47 ± 13	3.8843
	Pd	Cu	Ag	Mo		
	85.0	5.0	–	10.0		
	Measured value					
	Pd	Cu	Ag	Mo		
	84.6	5.8	–	9.6		

Table 2. Segregation in the near-surface region as measured by XPS.

Alloy	Condition	Composition [at%]			
		Pd	Cu	Ag	Mo
Pd-Cu-Ag	Before segregation	63.1	28.6	8.3	
	800 K in vacuum	57.8	22.5	19.7	
	1000 K in vacuum	58.3	25.4	16.3	
	800 K in 1 bar H_2	57.7	17.4	24.9	
	1000 K in 1 bar H_2	55.5	17.2	27.3	
Pd-Cu-Mo	Before segregation	87.4	4.3		8.3
	800 K in vacuum	87.4	4.0		8.6
	1000 K in vacuum	85.5	7.1		7.4
	800 K in 1 bar H_2	90.1	4.7		5.2
	1000 K in 1 bar H_2	88.8	4.6		6.6

elements nor oxide phases were observed. The grain size of the samples was estimated to be around 50 nm using the Williamson–Hall plot analysis.

3.2. Segregation of Near-Surface Region by XPS

By comparing the XPS results before and after annealing, the segregation trend in the near-surface region can be investigated. The XPS results in **Table 2** show that a hydrogen gas atmosphere definitely has an effect on the segregation in the near-surface region. Specifically, for Pd-Cu-Ag ternary alloy, there is a strong segregation of Ag in both vacuum and hydrogen, yet quantitatively the difference is about 5–10%. Similar results have been reported by Tarditi and Cornaglia,[20] although the atmosphere is not the same as in our work. However, for Pd-Cu-Mo ternary alloy, irrespective of the environment, i.e., in vacuum or in hydrogen gas, the change of Cu and Mo fraction in the outermost atomic layer is less than 3%. The annealing temperature also affects the surface composition, but the segregation trend remains unchanged.

3.3. Segregation of Outermost Atomic Layer by LEISS

Segregation of the outermost atomic layer was characterized by LEISS and the results are shown in **Figure 1**. By normalizing and multi-peak fitting, the elemental composition of the samples before and after segregation can be calculated with[35]

$$x_{\mathrm{A}}^{\mathrm{surf}} = \frac{I_{\mathrm{A}}}{I_{\mathrm{A}} + f_{\mathrm{A/B}} \cdot I_{\mathrm{B}} + f_{\mathrm{A/M}} \cdot I_{\mathrm{M}}} \tag{15}$$

where I_{A}, I_{B}, and I_{M} are intensities of the peaks corresponding to the scattering of atoms A, B, and M at the surface. $f_{\mathrm{A/M}}$ and $f_{\mathrm{A/M}}$ are the ratios of the scattered intensities of the corresponding pure metals.

In order to express the segregation trend, the composition change before and after segregation ($\Delta x_i = x_i^{\mathrm{after}} - x_i^{\mathrm{before}}$) of each element was calculated and is shown in **Figure 2**. The hydrogen gas atmosphere completely reverses the segregation in the outermost atomic layer of Pd-Cu-Ag ternary alloy. There is co-segregation of Cu and Ag in vacuum, but a strong segregation of Pd in 1 bar H_2 gas. However, for the Pd-Cu-Mo alloy, Pd segregation is observed in both vacuum and 1 bar H_2 gas, the atomic fraction of Mo is reduced, while that of Cu is barely changed. In contrast with the XPS results, LEISS data suggest that the segregation in the outermost atomic layer is not following the same trend with that in the near-surface region. Furthermore, segregation at 1000 K for 1 h is always stronger than at

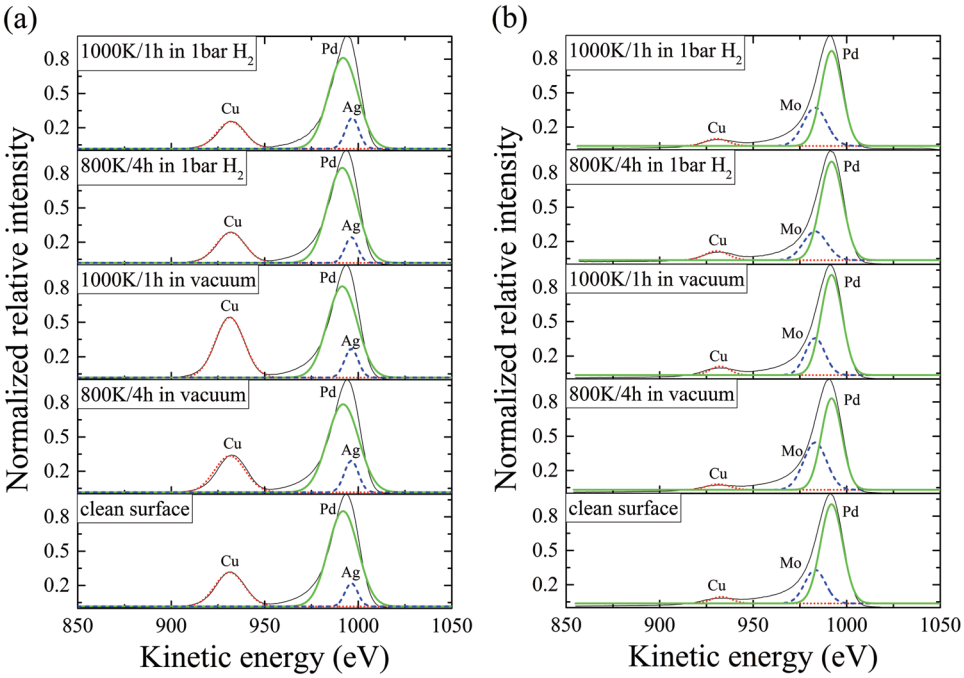

Figure 1. LEISS results of a) Pd-Cu-Ag and b) Pd-Cu-Mo ternary alloys (dotted line Cu, solid line Pd, dashed line Ag or Mo).

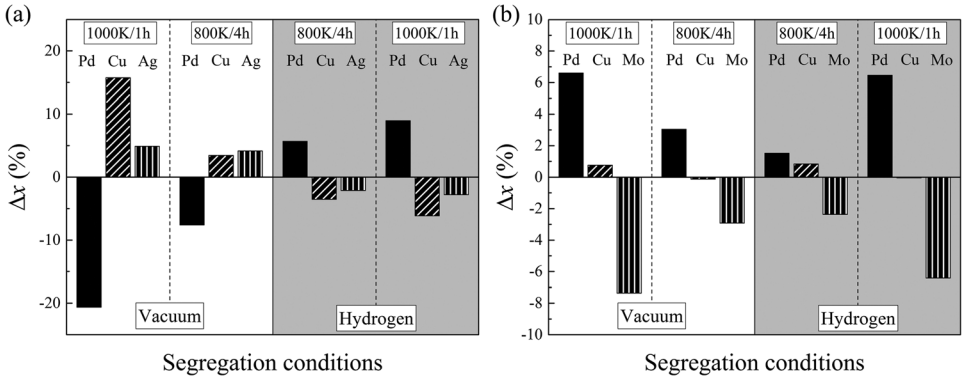

Figure 2. Composition change ($\Delta x = x^{after} - x^{before}$) of the outermost atomic layer of a) Pd-Cu-Ag ternary alloy and b) Pd-Cu-Mo ternary alloy.

800 K for 4 h, which is related to the kinetics of atomic diffusion. The experimental results reveal that the surface composition is still changing slowly after annealing at 800 K for 4 h, while it is stable after annealing in 1000 K for 1 h. Thus, at 800 K for 4 h the system did not reach equilibrium.

4. Discussion

4.1. Calculation of Surface Segregation in Vacuum

By the model proposed in Section 2, the elemental composition of the outermost atomic layer of the two investigated alloys upon segregation in vacuum is calculated first. As shown in **Table 3**, the calculation predicts co-segregation of Cu and Ag in the Pd-Cu-Ag ternary alloy, while it predicts segregation of Pd in the Pd-Cu-Mo ternary alloy. The surface orientation will not change the trend of segregation, it only has a slight influence on the composition, i.e., the difference between the calculated surface composition for the (111), (110), and (100) planes is less than 3%. The calculations also show that the higher the temperature, the less the segregation, which is because of the entropy effect in the Langmuir–McLean segregation equation (Equation (1)).

Table 3. Comparison between the calculated and experimental results for surface segregation of the outermost atomic layer in vacuum at corresponding temperatures. The segregation enthalpies are also listed. Theoretically, negative enthalpies lead to solute segregation, while positive enthalpies lead to solvent segregation.

Alloy	Condition	Calculation [at%]			Experiment result [at%]		
		Cu	Ag	Mo	Cu	Ag	Mo
Pd-Cu-Ag	Before segregation	30.0	10.0		29.4	10.4	
	800 K in vacuum	58.5	18.4		32.8	14.5	
	1000 K in vacuum	54.4	16.5		45.1	15.3	
	800 K in 1 bar H_2	29.2	3.2		25.9	8.2	
	1000 K in 1 bar H_2	29.9	3.9		23.2	7.6	
Pd-Cu-Mo	Before segregation	5.0		10.0	5.2		10.9
	800 K in vacuum	0		0	5.1		8.0
	1000 K in vacuum	0		0	6.0		3.6
	800 K in 1 bar H_2	0		0	6.0		8.5
	1000 K in 1 bar H_2	0		0	5.2		4.5

Alloy	Condition	Segregation enthalpy [kJ mol^{-1}]		
		Cu	Ag	Mo
Pd-Cu-Ag	800 K in vacuum	−10.8	−10.4	
	1000 K in vacuum	−11.0	−10.1	
Pd-Cu-Mo	800 K in vacuum	30.4		58.0
	1000 K in vacuum	30.4		57.8

Since segregation might be limited by the diffusion kinetics at 800 K as mentioned above, the experimental results at 1000 K were used to compare with our model predictions. As can be seen in Table 3, qualitatively our model provides good prediction for the Pd-Cu-Ag ternary alloy, i.e., co-segregation of Cu and Ag. Quantitatively, the surface atomic fraction of Ag is well-predicted, while that of Cu is higher than the experimental result. For the Pd-Cu-Mo ternary alloy, the model predicts that no Cu or Mo will be present in the outermost atomic layer, which is much lower than the observed composition.

In order to extend the scope of the discussion, the calculation was made for a wider range of compositions. For example, the surface composition of Pd-Cu-Ag alloy upon segregation is shown in **Figure 3**, in which the atomic fraction of Cu and Ag ranges from 5% to 30%. Clearly, there is a substantial effect of the bulk composition on the segregation of Cu and Ag. The increase of the bulk atomic fraction of one solute element reduces the surface atomic fraction of the other solute element. On the other hand, the surface segregation of Pd-Cu-Mo alloy was also calculated within the atomic fraction range of 1–10% for Cu and Mo. However, the surface fractions of Mo and Cu are always close to zero. Clearly, the surface segregation of the two solute elements in ternary alloys is not always independent but can strongly influence each other.

4.2. Comparison between the Surface Segregation of Binary and Ternary Alloys

For binary alloys, the reduction of the surface energy is the most important driving force of surface segregation, which indicates that the element with lower surface energy usually tends to segregate to the surface, although the elastic strain energy and chemical bonding energy are also of influence.[36]

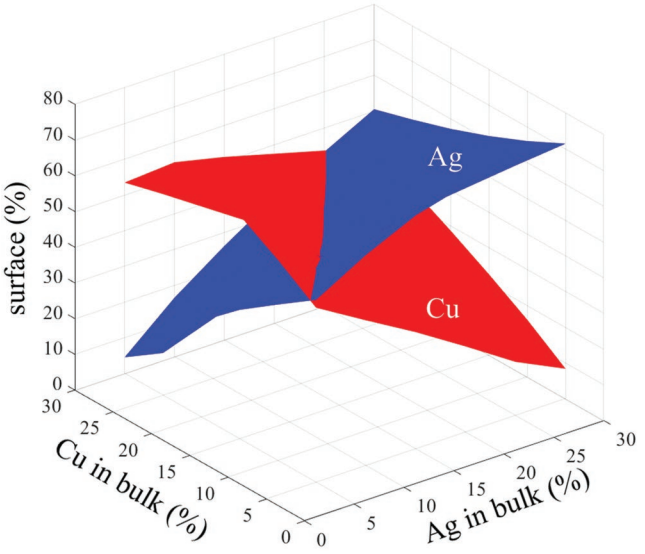

Figure 3. Surface segregation of Pd-Cu-Ag in a wider range of compositions in vacuum calculated at 1000 K.

For example, in the Pd-Ag and Pd-Cu binary alloys, the segregation of Ag and Cu in vacuum have been proven by experiments, while Pd segregation in the Pd-Mo binary alloys has also been predicted due to the much higher surface energy of Mo.[23,37,38] However, as mentioned above, the interaction between two solute elements makes the situation much more complicated in ternary alloys.

In general, the interaction, either attractive or repulsive, between two kinds of solute elements results in different segregation behaviors in ternary alloys: co-segregation, site-competition, and blocking.[27] Theoretically, an attractive atomic interaction may lead to co-segregation or blocking, as two kinds of solute element atoms prefer to be "together," while a repulsive atomic interaction may lead to site-competition, since they prefer to be "separate."

In order to understand the effect of solute interaction on the surface segregation of Pd-Cu-Ag and Pd-Cu-Mo ternary alloys, surface segregation of the related sub-binary alloys was also calculated at 1000 K in vacuum. As shown in **Table 4**, the segregation of Cu is moderately enhanced, and the segregation of Ag is strongly suppressed in Pd-Cu-Ag ternary alloy in contrast with Pd-Cu and Pd-Ag binary alloys with the same solute

Table 4. Comparison between the calculated surface segregation of the outermost atomic layer in binary and ternary alloys in vacuum at 1000 K.

Alloy	Before segregation [at%]				After segregation [at%]			
	Pd	Cu	Ag	Mo	Pd	Cu	Ag	Mo
Pd-Cu-Ag	60.0	30.0	10.0		29.1	54.4	16.5	
Pd-Cu	70.0	30.0			51.5	48.5		
Pd-Ag	90.0		10.0		64.3		35.7	
Pd-Cu-Mo	85.0	5.0		10.0	100	0		0
Pd-Cu	95.0	5.0			85.8	13.2		
Pd-Mo	90.0			10.0	100			0

fraction. This is clearly site-competition behavior, in which Cu atoms won more surface sites. This is also in agreement with the result shown in Figure 3. By contrast, Ag has lower surface energy and lower mixing enthalpy with Pd than Cu, both increase its segregation tendency. Therefore, the only possible reason of the site-competition result is the elastic strain energy. Since Pd and Ag have almost the same size and elastic moduli, the much larger elastic strain energy drives the Cu atoms to the surface. Note that Pd-Cu and Pd-Ag binary alloys are single phase with an FCC structure within 800–1000 K, but Cu-Ag binary alloys have a two-phase region, which may have some effect on the calculated results.[39–41]

For Pd-Cu-Mo, with 10 at% of Mo, Pd-Mo alloys form a single phase solid solution having an FCC structure.[42] In both Pd-Mo and Pd-Cu-Mo alloys, the model predicts that Mo has a strong preference to remain in the bulk, which can mainly be attributed to its much higher surface energy.[3] However, the calculation shows that less Cu will be at the surface upon segregation in the Pd-Cu-Mo ternary alloy. A possible explanation is the large positive mixing enthalpy of Cu-Mo. According to the phase diagram, Cu and Mo are completely immiscible below 1350 K.[43] Furthermore, the atom fraction of Cu and Mo is 5% and 10% in the Pd-Cu-Mo ternary alloy, which is lower than the 30 at% Cu and 10 at% Ag in the Pd-Cu-Ag ternary alloy. Therefore, Cu and Mo atoms may not be randomly distributed in the Pd matrix, which means that the interaction between Cu and Mo is likely overestimated in our calculations.

In our model, the solute interaction in ternary alloys is accounted for by ω_{AB} in Equation (3). As a simple approximation, a proportional factor is introduced to evaluate the effectiveness of Cu–Mo interaction on the surface segregation

$$\omega_{AB}^{\text{effective}} = \chi \cdot \omega_{AB} \, (0 \le \chi \le 1) \tag{16}$$

Clearly, a smaller χ corresponds to less interaction between the solute elements. Thus, $\chi = 0$ represents a mixture and random distribution, while $\chi = 1$ corresponds to strong interaction between two solute elements.

As shown in **Table 5**, χ indeed has a strong influence on the surface atomic fraction of Cu upon segregation. When $\chi = 0$ and 0.25, the calculation suggests segregation of Cu, which is in agreement with our experimental results; when $\chi > 0.25$, the interplay between segregation of Cu and Mo is overestimated, therefore the calculation suggests no Cu at the surface. It can be concluded that the atomic interaction between solute elements and the interplay between their segregation have a significant effect on the surface segregation of ternary alloys. For different ternary alloys, this effect can also be quite different. Notably, χ here is a fitting parameter.

4.3. Effect of Hydrogen Atmosphere on the Surface Segregation

Segregation of ternary alloys in hydrogen atmosphere was also calculated for 1000 K. In order to separately discuss the effect of hydrogen adsorption on the surface as well as the absorption in the bulk, two series of situations are considered; first the adsorption coverage θ and next the absorption concentration x_H

Table 5. Effect of solute interaction parameter χ on the surface segregation.

Condition		Pd-Cu-Mo		Pd-Cu-Ag	
		Cu [at%]	Mo [at%]	Cu [at%]	Ag [at%]
Before segregation		5.0	10.0	30	10
After segregation	$\chi = 1$	0	0	54.4	16.5
	$\chi = 0.75$	0.6	0	54.2	15.1
	$\chi = 0.5$	2.0	0	54.8	13.7
	$\chi = 0.25$	5.8	0	56.6	11.9
	$\chi = 0$	14.2	0	61.3	9.6

were varied independently. In view of the results in vacuum, see Section 3.2, $\chi = 0.25$ is chosen again for the calculations for the Pd-Cu-Mo ternary alloy.

The effect of hydrogen adsorption was first considered without absorption ($x_H = 0$). As shown in **Figure 4**a,c, the increase of hydrogen adsorption ($0 \le \theta \le 1$) can enhance the segregation of Pd in both alloys, leading to lower atomic fractions of solute elements in the outermost atomic layer. This is mainly because of the higher adsorption energy of H atoms on Pd than on the solute elements.[44] Furthermore, hydrogen absorption ($0 \le x_H \le 0.2$) was additionally considered on the basis of $\theta = 0.5$, corresponding to the half-covered adsorption. It also increases the surface atomic fraction of Pd, as shown in Figure 4b,d. In summary, segregation trends of Cu and Ag are reversed in a hydrogen gas atmosphere for both ternary alloys, while the atomic fraction of Mo remains almost 0 at various conditions.

According to the literature about metal-hydrogen phase diagram, there would be almost no hydrogen absorption ($x_H < 0.01$) in Pd-Cu-Ag and Pd-Cu-Mo ternary alloys at 1 bar H_2 gas pressure and at temperatures within the range of 800–1000 K.[45,46] Therefore, it can be concluded that hydrogen adsorption on the surface reverses the segregation behavior of Cu and Ag in the Pd-Cu-Ag ternary alloy by increasing the Pd atomic fraction of the surface. This is in good agreement with the experimental results; see Figure 2. The effect of hydrogen adsorption on the segregation behavior of Pd-Cu-Mo ternary alloy is small, since Pd segregation is already occurring in vacuum.

4.4. Depth Profile Analysis of the Surface Segregation

The depth profile of surface segregation can be evaluated by comparing the XPS and LEISS results; see Tables 2 and 3. It is quite obvious that the trend of segregation in the near-surface region and the outermost atomic layer of ternary alloys is not always the same, especially for Pd-Cu-Ag in the present work. The LEISS results show a co-segregation of Cu and Ag on the outermost atomic layer. However, XPS with an analysis depth of about ten atomic layers indicates that there is only segregation of Ag in this region. The atomic fraction of Cu is even lower than that in the bulk. This can be explained again by the

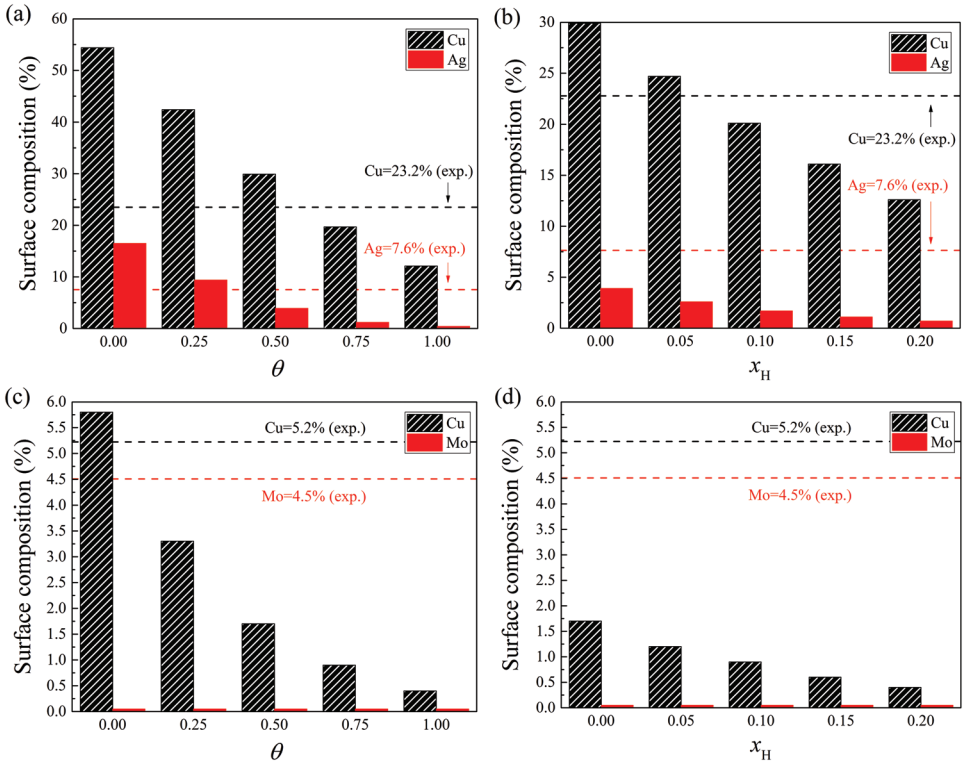

Figure 4. Composition of the outermost atomic layer upon segregation at 1000 K in hydrogen atmosphere: a) Pd-Cu-Ag, $0 \le \theta \le 1$, $x_H = 0$; b) Pd-Cu-Ag, $\theta = 0.5$, $0 \le x_H \le 0.2$; c) Pd-Cu-Mo, $0 \le \theta \le 1$, $x_H = 0$; d) Pd-Cu-Mo, $\theta = 0.5$, $0 \le x_H \le 0.2$. As a comparison, the experimental results are also shown; see the dash lines.

site-competition behavior. For Pd-Cu and Pd-Ag sub-binary alloys, both Cu and Ag tend to segregate to the surface. As a result, both Cu and Ag are rich in the near-surface region as a "sub-surface layer."[47,48] Then, the experimental result suggests that there is an additional step of segregation in this layer, in which Cu occupies more sites on the outermost atomic layer by exchanging with Ag underneath. Consequently, there are a Cu-rich outermost atomic layer and an Ag-rich in the near-surface region, which fits perfectly with our experimental results. This phenomenon is not noticeable for Pd-Cu-Mo ternary alloys since the segregation is not so strong as in the Pd-Cu-Ag ternary alloy.

4.5. Application of the Model to Other Ternary Alloys

Ternary alloys are widely used and surface segregation is a common phenomenon in these alloys. In order to verify the model proposed, the surface segregation behavior of four other ternary alloys is also predicted. The results are compared with experimental or computational results from publications, as listed in **Table 6**.[27,49–51] The calculations were performed at the temperatures reported in the corresponding literature and using the same crystal structure. Specifically, Fe-Cr-Ni, Cu-Ag-Au, and Pt-Pd-Rh alloys have FCC structure at the corresponding temperature, while Ni-Al-Cu has a BCC structure. The segregation behaviors predicted by our model are in good agreement with the results reported in literature, while quantitatively, specific surface compositions upon segregation show some differences with the experimental results. Notably, some of the characterizing methods may not measure the composition of the outermost atomic layer. In general, our model can be used as a semiquantitative method to predict the surface segregation behavior of single-phase ternary solid solutions.

5. Conclusion

Surface segregation of Pd-Cu-Ag and Pd-Cu-Mo ternary alloys was experimentally investigated by XPS and LEISS in both vacuum and hydrogen atmosphere. A thermodynamic model was proposed to understand and enable prediction of segregation behavior in ternary alloys. In vacuum, interaction between the two solute elements is proven to have a strong impact on the segregation behavior. Site-competition of Cu and Ag is observed in a Pd-Cu-Ag ternary alloy, leading to a different trend of segregation in the near-surface region and on the outermost atomic layer. Whereas the influence between the segregation of Cu and Mo in Pd-Cu-Mo ternary alloy is limited due to the relatively weak interaction between Cu and Mo. In a hydrogen gas atmosphere, it is the hydrogen adsorption on the surface that reverses the surface composition from solute segregation in vacuum to Pd segregation. These results provide basic guidelines to design hydrogen separation membranes with better surface stability. The proposed thermodynamic model for the surface segregation of ternary alloys is generic and thus can be applied to predict the segregation behavior of other single-phase ternary alloys.

Table 6. Comparison between the calculated and literature reported results for surface segregation in several ternary alloys.[26,48–50] The compositions are given in atomic percent of the corresponding element in the alloy.

Alloy	Temperature	Literature method	Surface composition	
			Literature	Calculation (in this work)
Fe72-Cr20-Ni8	723 K	Atom probe	Fe52Cr34Ni 14	Fe62Cr29Ni9
Cu92-Ag1-Au7	800 K	AES[a)]	Cu13Ag85Au2	Cu78Ag20Au4
Ni50-Al40-Cu10	1000 K	Monte Carlo	Ni0Al62Cu38	Ni2Al87Cu11
Pt83-Pd15-Rh2	1200 K	Monte Carlo	Pt74Pd26Rh0	Pt47Pd52Rh1

[a)]Notably, AES may not measure the composition of the outermost atomic layer.

6. Experimental Section

The surface segregation of Pd-Cu-Ag and Pd-Cu-Mo ternary alloys was experimentally investigated. The samples were manufactured (Chempur, Karlsruhe, Germany) by arc-melting and cold-rolling yielding a thickness of 100 µm and nominal compositions as listed in Table 1. The surface was polished by an oxide polishing suspension with a particle size of 0.05 µm. The actual bulk composition of the samples was determined with X-ray microanalysis (XMA) using EDS (Thermo Fischer Noran System 7, USA) in an SEM (JEOL JSM 6500F, Tokyo, Japan). The samples were characterized by XRD (Bruker AXS GmbH D8, Karlsruhe, Germany; 50 kV, 1000 mA, Cu kα radiation, 1.5406 Å). Lattice constants of the samples are also listed in Table 1 and no impurity phases could be detected.

A clean surface of the samples was obtained by Ar^+ ion sputtering and short-time recovery at 800 K for 60 min in UHV chamber (base pressure < 10^{-7} Pa). XPS and LEISS (Perkin Elmer PHI 5400 ESCA, Eden Prairie, USA) were used to determine the initial elemental composition of the clean surface. Then the samples were transferred under vacuum to the annealing chamber and annealed at 800 K for 4 h and 1000 K for 1 h, respectively, to evoke surface segregation, in both vacuum and 1 bar H_2. The heating was realized by focused white light to eliminate the contaminations from heating units in common furnaces. The cooling rate was in the range of 100 K min^{-1}, therefore diffusion during cooling process could be ignored. After cooling down, the samples were transferred back to the XPS analysis chamber and the surface composition upon segregation was measured. Specifically, the spectra were obtained using a nonmonochromatic Al Kα radiation at 200 W and 13.1 kV. The main photoelectron lines of each element in the samples (Pd 3d, Cu 2p, Ag 3d, and Mo 3d) were recorded with a step size of 0.5 eV and a dwell time of 100 ms using a spherical capacitor analyzer set with a pass energy of 71.55 eV. The photoelectrons were observed with the analyzer input lens at 45° with respect to the sample surface normal. Then, the composition was quantified from the peak area of the photoelectron lines after Shirley background subtraction and adopting the corresponding sensitivity factors. XPS gave compositional information coming mainly from a depth of the inelastic mean free path, which is 10–20 Å for related elements, corresponding to about ten atomic layers.[20] LEISS spectra were taken with 1 keV $^3He^+$ incidence with a low current of 500 nA to minimize the ion bombardment. Then, the elemental composition of the outermost atomic layer could be determined by the intensity of Gaussian-fitted peaks corresponding with each element. By comparing the surface composition before and after annealing, the surface segregation in vacuum and hydrogen was determined.

Supporting Information

Supporting Information is available from the Wiley Online Library or from the author.

Acknowledgements

The authors acknowledge the financial support from ADEM, A green Deal in Energy Materials of the Ministry of Economic Affairs of The Netherlands (www.adem-innovationlab.nl). The authors also thank Ing. Ruud W.A. Hendrikx for the XRD measurement and analysis.

Conflict of Interest

The authors declare no conflict of interest.

Keywords

LEISS, surface segregation, ternary alloys, thermodynamic modeling

Received: October 22, 2019
Revised: December 28, 2019
Published online:

[1] M. Kranzberg, C. S. Smith, *Mater. Sci. Eng.* **1979**, *37*, 1.
[2] S. Srinivasan, S. Ranganathan, *Trans. Indian Inst. Met.* **2006**, *59*, 829.
[3] F. R. de Boer, R. Boom, W. C. M. Mattens, A. R. Miedema, A. K. Niessen, *Cohesion in Metals*, Elsevier Science Publishers, New York **1988**.
[4] P. L. Mangonon, G. Thomas, *Metall. Trans.* **1970**, *1*, 1577.
[5] M. Hattori, N. Goto, Y. Murata, T. Koyama, M. Morinaga, *Mater. Trans.* **2005**, *46*, 163.
[6] P. A. Fedders, M. W. Muller, *J. Phys. Chem. Solids* **1984**, *45*, 685.
[7] C. Wang, D. Li, M. Chi, J. Pearson, R. B. Rankin, J. Greeley, Z. Duan, G. Wang, D. Vliet, K. L. More, N. M. Markovic, V. R. Stamenkovic, *J. Phys. Chem. Lett.* **2012**, *3*, 1668.
[8] A. Seo, J. Lee, K. Han, H. Kim, *Electrochim. Acta* **2006**, *52*, 1603.
[9] L. Zhao, A. Goldbach, C. Bao, H. Xu, *ACS Appl. Mater. Interfaces* **2014**, *6*, 22408.
[10] B. D. Adams, A. Chen, *Mater. Today* **2011**, *14*, 282.
[11] F. A. Lewis, *Int. J. Hydrogen Energy* **1996**, *21*, 461.
[12] S. Tosti, A. Basile, L. Bettinali, F. Borgognoni, F. Gallucci, C. Rizzello, *Int. J. Hydrogen Energy* **2008**, *33*, 5098.
[13] S. Yun, S. T. Oyama, *J. Membr. Sci.* **2011**, *375*, 28.
[14] N. I. Timofeev, F. N. Berseneva, V. M. Makarov, *Int. J. Hydrogen Energy* **1994**, *19*, 895.
[15] S. Tosti, L. Bettinali, V. Violante, *Int. J. Hydrogen Energy* **2000**, *25*, 319.
[16] H. Jia, A. Goldbach, C. Zhao, G. R. Castro, C. Sun, H. Xu, *J. Membr. Sci.* **2017**, *529*, 142.
[17] J. Shu, B. E. W. Bongondo, B. P. A. Grandjean, A. Adnot, S. Kaliaguine, *Surf. Sci.* **1993**, *291*, 129.
[18] T. Lai, M. L. Lind, *Int. J. Hydrogen Energy* **2015**, *40*, 373.
[19] A. M. Tarditi, F. Braun, L. M. Cornaglia, *Appl. Surf. Sci.* **2011**, *257*, 6626.
[20] A. M. Tarditi, L. M. Cornaglia, *Surf. Sci.* **2011**, *605*, 62.
[21] A. M. Tarditi, C. Imhoff, J. B. Miller, L. M. Cornaglia, *Surf. Interface Anal.* **2015**, *47*, 745.
[22] D. Tomanek, S. Mukherjee, V. Kumar, K. H. Bennemann, *Surf. Sci.* **1982**, *114*, 11.
[23] M. Zhao, W. G. Sloof, A. J. Böttger, *Int. J. Hydrogen Energy* **2018**, *43*, 2212.
[24] M. Guttmann, *Surf. Sci.* **1975**, *53*, 213.
[25] M. A. Hoffmann, P. Wynblatt, *Metall. Trans. A* **1989**, *20*, 215.
[26] A. A. B. Padama, H. Kasai, Y. W. Budhi, *Int. J. Hydrogen Energy* **2013**, *38*, 14715.
[27] J. Luyten, C. Creemers, *Surf. Sci.* **2008**, *602*, 2491.
[28] Y. Chen, S. Liao, H. Deng, *Appl. Surf. Sci.* **2007**, *253*, 6074.
[29] T. B. Flanagan, C. Park, *J. Alloys Compd.* **1999**, *293–295*, 161.
[30] G. Maire, L. Hilaire, P. Legare, F. G. Gault, A. O'cinneide, *J. Catal.* **1976**, *44*, 293.
[31] P. K. Ray, M. Akinc, M. J. Kramer, *J. Alloys Compd.* **2010**, *489*, 357.
[32] B. Zhang, W. A. Jesser, *Phys. B* **2002**, *315*, 123.
[33] Y. Ouyang, X. Zhong, Y. Du, Z. Jin, Y. He, Z. Yuan, *J. Alloys Compd.* **2006**, *416*, 148.
[34] W. C. Wang, J. H. Li, H. F. Yan, B. X. Liu, *Scr. Mater.* **2007**, *56*, 975.
[35] C. W. Yi, K. Luo, T. Wei, D. W. Goodman, *J. Phys. Chem. B* **2005**, *109*, 18535.
[36] P. Wynblatt, R. C. Ku, *Surf. Sci.* **1977**, *65*, 511.
[37] P. T. Wouda, M. Schimid, B. E. Nieuwenhuys, P. Varga, *Surf. Sci.* **1998**, *417*, 292.
[38] D. Priyadarshini, P. Kondratyuk, Y. N. Picard, B. D. Morreale, A. J. Gellman, J. B. Miller, *J. Phys. Chem. C* **2011**, *115*, 10155.
[39] M. Li, Z. Du, C. Guo, C. Li, *Calphad* **2008**, *32*, 439.
[40] I. Karakaya, W. T. Thompson, *Bull. Alloy Phase Diagrams* **1988**, *9*, 237.
[41] P. L. Williams, Y. Mishin, J. C. Hamilton, *Modell. Simul. Mater. Sci. Eng.* **2006**, *14*, 817.
[42] G. Ghosh, G. B. Olson, *J. Phase Equilib.* **2000**, *21*, 32.
[43] P. R. Subramanian, D. E. Laughlin, *Bull. Alloy Phase Diagrams* **1990**, *11*, 169.
[44] P. Nordlander, S. Holloway, J. K. Norskov, *Surf. Sci.* **1984**, *136*, 59.
[45] F. D. Manchester, A. San-Martin, J. M. Pitre, *J. Phase Equilib.* **1994**, *15*, 62.
[46] S. Nayebossadri, J. D. Speight, D. Book, *ACS Appl. Mater. Interfaces* **2017**, *9*, 2650.
[47] J. Greeley, M. Mavrikakis, *Nat. Mater.* **2004**, *3*, 810.
[48] M. Engelke, B. Schonfeld, *Acta Mater.* **2013**, *61*, 5087.
[49] K. Takahashi, Y. Ishikawa, T. Yoshimura, O. Nishikawa, *J. Phys. Colloq.* **1986**, *47*, C7.
[50] M. A. Hoffmann, P. Wynblatt, *Metall. Trans. A* **1991**, *22*, 1833.
[51] F. S. Honecy, G. Bozzolo, B. Good, *Appl. Surf. Sci.* **1999**, *137*, 157.